ACS APPLIED MATERIALS & INTERFACES

Research Article

www.acsami.org

Facile Synthesis of Nitrogen-Doped Graphene–Ultrathin MnO_2 Sheet Composites and Their Electrochemical Performances

Shuhua Yang, Xuefeng Song,* Peng Zhang, and Lian Gao*

State Key Laboratory for Metallic Matrix Composite Materials, School of Materials Science and Engineering, Shanghai Jiao Tong University, Shanghai, 200240, China

Supporting Information

ABSTRACT: Nitrogen-doped graphene–ultrathin MnO_2 sheet composites (NGMCs) were prepared through a one-step hydrothermal method at low temperature (120 °C). Ultrathin MnO_2 sheets were well-dispersed and tightly anchored on graphene sheets, which were doped with nitrogen simultaneously. NGMCs electrode exhibited enhanced capacitive performances relative to those of undoped graphene-ultrathin MnO_2 sheets composites (GMCs). As the current density increased from 0.2 to 2 A/g, the capacitance of NGMCs still retained ~74.9%, which was considerablely higher than that of GMCs (27%). Moreover, over 94.2% of the original capacitance was maintained after 2000 cycles, indicating a good cycle stability of NGMCs electrode materials.

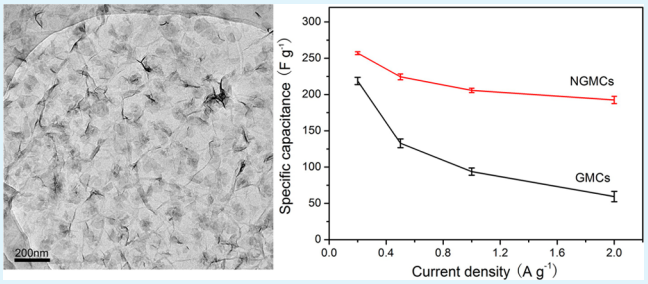

KEYWORDS: *nitrogen-doped graphene, ultrathin MnO_2 sheets, surface active sites, electrode materials, supercapacitors*

INTRODUCTION

The fast depletion of fossil fuels and pollution of the environment has caused an ever increasing demand for a sustainable and renewable energy storage system. Among the various energy storage systems, supercapacitors are considered promising candidates for effective energy storage because of their high power density, rapid charging–discharging rates, long cycle life, and low maintenance cost.[1−3]

MnO_2 is one of the most promising pseudocapacitive materials for its high-energy density, low cost, environmental compatibility, and natural abundance.[4−6] Over the past few years, various MnO_2 nanostructures have been successfully synthesized and used as electrodes for supercapacitor.[7−9] However, the poor conductivity of MnO_2 (~1×10^5 S/cm) limits its applications in high-performance supercapacitors. In order to enhance the electrical conductivity of MnO_2 electrodes, tremendous efforts have been focused on combining highly conductive materials such as graphene, carbon nanotubes, porous carbon, and activated carbons.[10−13] Among these materials, graphene, a single layer of two-dimensional carbon atoms, has received significant attention owing to its extraordinary electrical conductivity, high surface area, and good mechanical properties.[14−17] Chen et al. have reported that GO/MnO_2 nanocomposites could be employed as electrode material with excellent electrochemical behaviors for supercapacitor.[18] Zhu et al. have investigated graphene-wrapped MnO_2 nanocomposites, which exhibited enhanced capacitive performance as high as 210 F/g at 0.5 A/g.[19] Although tremendous achievements have been made, a number of challenges still need to be addressed, such as the complexity of synthesis, poor cycling performance due to the poor connection between graphene and the pseudocapacitive material, and rate performance.

To open the potential applications of graphene-based materials and improve their electrochemical properties, a number of attempts have been focused on functionalized graphene.[20−22] Nitrogen doping has become a key-enabling technology to improve the properties of graphene through increasing its conductivity and surface active sites.[23] To date, most research relates to the synthesis and characterization of single phase of nitrogen-doped graphene (NG).[24−26] There are few reports on preparing NG-based composites with well-dispersed ultrathin MnO_2 sheets. Herein, we first develop a facile method to synthesize NG–ultrathin MnO_2 sheets composites (NGMCs) with excellent electrochemical properties for supercapacitor. The as-prepared NGMCs possess several advantages. First, NG enhances capacity and rate performance while maintaining the superb cycleability of a supercapacitor, because of the presence of pyrrolic nitrogen and the pyridinic nitrogen in graphene.[27,28] Second, the ultrathin MnO_2 sheets facilitate electrolyte transport, active site accessibility, and electron transportation between NG and ultrathin MnO_2 sheets. Third, the method can be easily scaled up and extended to fabricate other oxides/NG composites.

EXPERIMENTAL SECTION

Synthesis of NGMCs. All chemical reagents used in this study are of analytical grade, and used without further purification. Graphite

Received: January 29, 2013
Accepted: March 26, 2013
Published: March 26, 2013

   dx.doi.org/10.1021/am400385g | ACS Appl. Mater. Interfaces 2013, 5, 3317−3322

oxide (GO) was synthesized using natural graphite (Alfa Aesar, 325 mesh, 99.8%) according to modified Hummers method.[29] NGMCs were prepared by using a facile one-pot hydrothermal process. In a typical synthesis, 316 mg of $KMnO_4$ was added into 39 mL of homogeneous GO solution (1.2 mg/mL), followed by stirring for 15 min at room temperature. Then 1 g urea was added to the suspension. After vigorous agitation for another 15 min, the mixture solution was transferred into a 50 mL Teflon-lined stainless steel autoclave and heated at 120 °C for 12 h. The NGMCs were obtained after centrifugation washing with deionized water for several times, and then dried in a vacuum oven at 60 °C for 12 h. For comparison, graphene-ultrathin MnO_2 sheets composites (GMCs) were prepared by the same procedure in the absence of urea. A similar procedure was applied to prepare MnO_2 sheets except addition of urea and GO. Meanwhile, reduced graphene oxide (RGO) was synthesized by hydrothermal process.[30]

Characterizations. Samples were characterized using powder X-ray diffraction (XRD) on a Goniometer Ultima IV (185 mm) diffractometer with Cu Kα radiation (λ = 1.5418 Å) at a step of 0.01° per second. Morphologies of as-obtained products were observed on a field emission scanning electron microscopy (FESEM, FEI Sirion 200). Transmission electron microscopy (TEM) images were achieved on a JEOL JEM-2010F transmission electron microscope operated at an acceleration voltage of 200 kV. Raman spectra were taken on a DXR Raman Microscope with an excitation length of 532 nm. X-ray photoelectron spectroscopic measurements were performed on a Kratos AXIS Ultra DLD spectrometer. Thermogravimetric analyses (TGA) were run on a SDT Q600 V20.9 Build 20 thermogravimetric analyzer at a heating rate of 10 °C min^{-1} from 50 to 850 °C in air. Nitrogen adsorption/desorption isotherms were measured on an ASAP 2010 M+C surface area and porosimetry analyzer at 77 K.

Preparation of Electrodes and Electrochemical Measurements. The working electrodes were fabricated as follows. Briefly, the as-prepared materials, acetylene black and polyvinylidene difluoride (PVDF) were mixed in a mass ratio of 80:15:5 and dispersed in N-methyl pyrrolidone (NMP) solvent. The resulting slurry was coated onto the nickel foam substrate (1 cm ×1 cm) with a spatula, followed by drying at 60 °C for 12 h. Finally, the electrode was pressed under a pressure of 10 MPa. All electrochemical measurements were carried out by a three-electrode experimental setup (CHI660D electrochemical workstation, Chenhua, Shanghai), in which a platinum wire and a saturated calomel electrode (SCE) were used as the counter and reference electrode, respectively. A 1 M Na_2SO_4 was used as electrolyte.

RESULTS AND DISCUSSION

Microstructure Characterizations. Representative X-ray diffraction (XRD) patterns of RGO, MnO_2 sheets, GMCs and NGMCs are shown in Figure 1a. For sample RGO, two characteristic diffraction peaks can be observed at 26.5 and 42.8°, corresponding to the (002) and (100) planes of graphene. For MnO_2 sheets, five observed diffraction peaks at around 12.8, 37.4, 41.8, 50, and 65.5° can be indexed to the (110), (211), (301), (411), and (002) reflection of α-MnO_2 (JCPDS No.44−0141), respectively. The XRD patterns of GMCs and NGMCs clearly show the poor crystallinity of MnO_2, which is likely attributed to the incorporation of graphene. The peak at 26.5°, resulting from graphene, suggests that urea is an effective reducing agent to reduce graphene oxide to graphene. Moreover, negligible differences observed in the spectra of both GMCs and NGMCs reveal that nitrogen doping has little influence on the average crystallite size of MnO_2 sheets.

The morphology and structure of the as-synthesized composites were investigated by using SEM and TEM (Figure 1b−f and Figure S1 in the Supporting Information). It can be seen that the MnO_2 with sheet-like shape is homogeneously

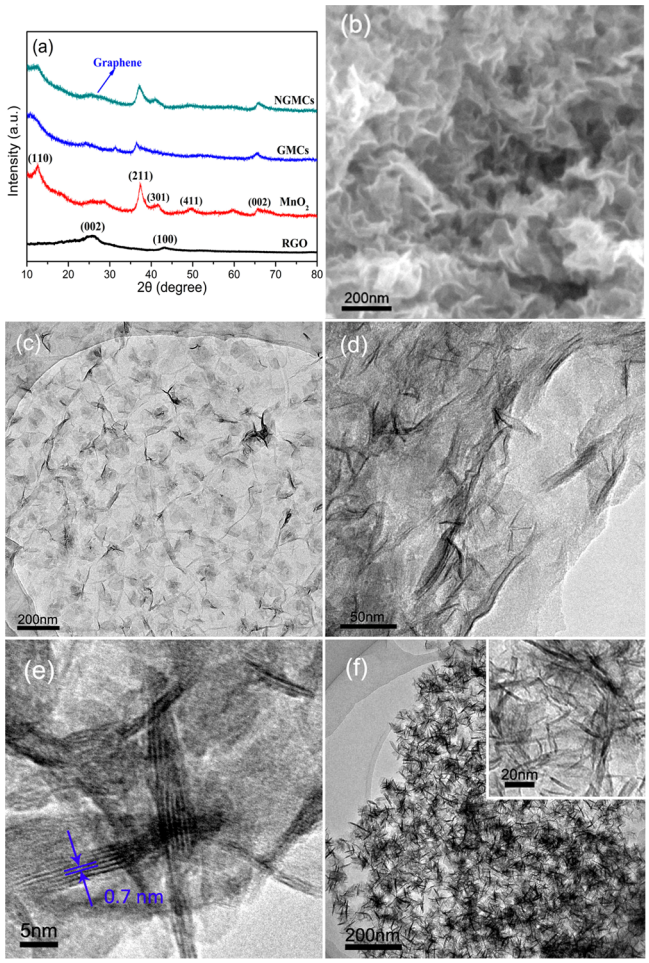

Figure 1. (a) XRD patterns of RGO, MnO_2, GMCs, and NGMCs, (b)SEM image of NGMCs, (c) low- and (d) high-magnification TEM image of NGMCs, (e) HRTEM image of the ultrathin MnO_2 sheets in NGMCs, and (f) TEM images of GMCs. The inset in f is the partial enlarged image of GMCs.

and tightly attached on the graphene surfaces (Figure 1b). TEM images further confirm that the as-prepared NGMCs are made of ultrathin MnO_2 sheets and transparent graphene thin films (Figure 1c and Figure S1a in the Supporting Information). Figure 1d shows that the ultrathin MnO_2 sheets have widths ranging from 3 to 10 nm and lengths up to about 100 nm (Figure S2 in the Supporting Information). The sheetlike MnO_2 was homogeneously decorated on graphene surface and partially covered the graphene surfaces, which is consistent with the SEM characterization. Meanwhile, it was found that the ultrathin MnO_2 sheets were tightly connected with doped graphene sheets even after sonication, which is favorable for the improvement of cycle life as an electrode for supercapacitor. The high resolution TEM (HRTEM) (Figure 1e) shows that the interplanar distances of lattice fringes are approximately 0.7 nm, which corresponds to the (110) plane of the tetragonal MnO_2 structure. Moreover, the selected area electron diffraction (SAED) pattern and HRTEM demonstrate that some amorphous MnO_2 ultrathin sheets were formed on the surface of graphene (Figure S3 in the Supporting Information), further confirming the poor crystallinity of MnO_2 sheets. It is believed that this amorphous structure is beneficial for the improvement of the electrochemical performance as a supercapacitor electrode.[31] For comparison, the morphology of

GMCs was also characterized using TEM. The sheetlike MnO_2 tends to agglomerate for the GMCs. This indicates that nitrogen doping might play a key role in homogeneous dispersion of ultrathin MnO_2 sheets on graphene surface, as shown in Figure 1f and Figure S1b in the Supporting Information. As shown by Chen et al.,[18] GO sheets have many oxygen-containing functional groups which act as anchoring sites for formation of MnO_2. During NGMCs preparation, a part of oxygen-containing functional groups have been removed by urea,[26] so NG has fewer anchoring sites than GO for formation of MnO_2. Therefore, NG sheets can load well-dispersed ultrathin MnO_2 comparing to the aggregation of MnO_2 sheets on RGO.

The typical Raman spectra of the RGO and NGMCs samples are displayed in Figure 2. The characteristic D and G band of

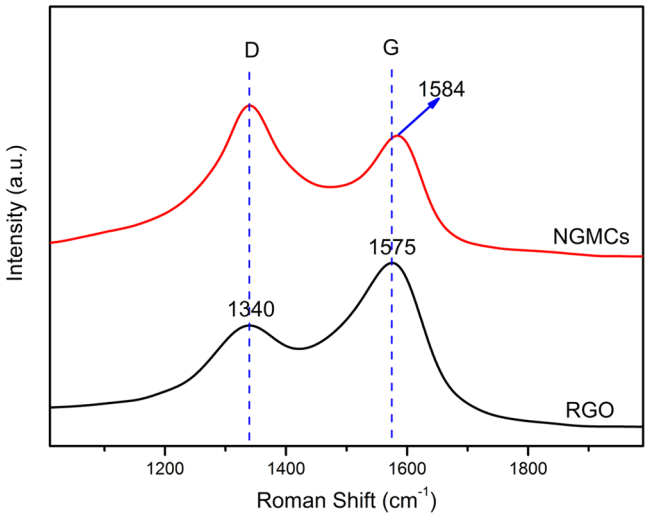

Figure 2. Raman spectra of NGMCs with 2.77 at % doping level and RGO.

RGO are observed at 1340 and 1575 cm^{-1}, respectively.[32] For NGMCs, the G band shifts to 1584 cm^{-1}, indicating insertions of N atoms in graphene.[33] Compared with RGO, the NGMCs exhibit strong D band peak at 1340 cm^{-1} due to a high defect density (incorporated N).[34] Furthermore, the NGMCs reveal higher intensity ratio of D band and G band (I_D/I_G) (1.09) than the pristine graphene (0.66), which is an indication of high concentration of structure defects on the surface of graphene sheets.[33] As we know, the defects of graphene can provide more active sites for electron storage, which can improve the capacitance of the composites.[35] The suitable defects of graphene derived from the N-configuration can improve capacitances of the NMGCs because of their enhanced binding energies with ions in the electrolyte. Because larger binding energy leads to a larger number of ions being accommodated on the electrode surface, the enhancement of binding energy would improve the capacitance.[35] Therefore, the composites are expected to be a promising candidate for high-capacitance electrodes materials for supercapacitor.

To investigate the as-prepared NGMCs in detail, the X-ray photoelectron spectroscopy (XPS) study was carried out to determine the electronic structure and compositions. As shown in Figure 3a, the survey spectrum shows that the as prepared composites contain Mn, C, O and N, which provides evidence for N doping in graphene lattices. The deconvoluted high-resolution N1s spectra of NGMCs are shown in Figure 3b. The XPS reveals that both pyridinelike (398.6 eV) and pyrrolic (399.8 eV) nitrogen atoms exist in the graphene structure.[36−38] The pyridinic nitrogen at graphene can provide a pair of electrons for conjugation with the π-conjugated rings; therefore, it can introduce electron donor properties to graphene sheets and improve the electrochemical performances of NGMCs.[27,39] The pyrrolic nitrogen have higher charge mobility in graphene due to better electron-donor characteristics and enhanced carbon catalytic activity in electron-transfer reactions, which plays key roles in the improved capacitances.[35,40] The content of element N in the product is calculated to be 2.77 atom %. It has been demonstrated that N doping can increase the electrical conductivity and electrochemical activity of graphene in the high-rate electrochemical process.[41] Thus, the NGMCs are expected to improve the high rate performance of electrode material in supercapacitor. The high-resolution spectrum of Mn 2p in Figure 3c obviously shows that the peaks centered at 642 and 653.6 eV can be assigned to Mn $2p_{3/2}$ and Mn $2p_{1/2}$ peaks, respectively, confirming the presence of MnO_2 in the composites.[42−45] In addition, the spectrum of O1s is depicted in Figure 3d. The deconvolution peaks of O 1s spectrum can be divided into two peaks centered at 529.6 and 531.3 eV, which corresponds to O−Mn bonding configuration and C−O bonding configuration, respectively.[46−49]

The chemical binding state of GMCs was also investigated by XPS. Figure S4 in the Supporting Information shows that there is no N 1s peak in the XPS spectrum of GMCs, which further indicates that the nitrogen atoms derived from urea can be doped into graphene for NGMCs by the hydrothermal process. The actual content of each component of as prepared NGMCs were investigated by TGA (Figure S5 in the Supporting Information). The NG prepared by thermal solid-state reaction[25] was also characterized by TGA for comparison, as shown in Figure S5 in the Supporting Information. The experiments were performed from 50 to 850 °C in air flow at a heating rate of 10 °C min^{-1}. In the process, the NG sheets were burned up, whereas MnO_2 turned into Mn_2O_3.[18,50] The weight loss of NG is 100% while the weight loss of NGMCs is 39.18%. On the basis of the above analysis, we can conclude that the mass ratio of MnO_2/NG can be derived to be 2.02/1 in the NGMCs.

On the basis of the above experimental results, it can be concluded that NGMCs were fabricated through a one step hydrothermal method. While MnO_2 was anchored on graphene surfaces, nitrogen doping was achieved simultaneously. According to eq 1, $KMnO_4$ can react with the graphene to form MnO_2 on the graphene surfaces.[11] In the preparation process of NGMCs, the urea plays a key role, which acts as both the nitrogen source and the reduction agent. As the nitrogen source, it is confirmed by the fact that no obvious nitrogen content was detected in a controlled experiment without urea (Figure S4 in the Supporting Information). Furthermore, as reported by Lei et al.,[26] urea is an effective reduction agent, which reduces the oxygen-containing functional groups on the GO surface.

$$4KMnO_4 + 3C + H_2O \rightarrow 4MnO_2 + K_2CO_3 + 2KHCO_3 \quad (1)$$

Electrochemical Behavior. The capacitive performances of NGMCs as electrode material for supercapacitor were evaluated by cycle voltammetry (CV) and galvanostatic charge/discharge techniques. Figure 4a shows the CV curves of NGMCs at different scan rates ranging from 5 to 100 mV/s in 1

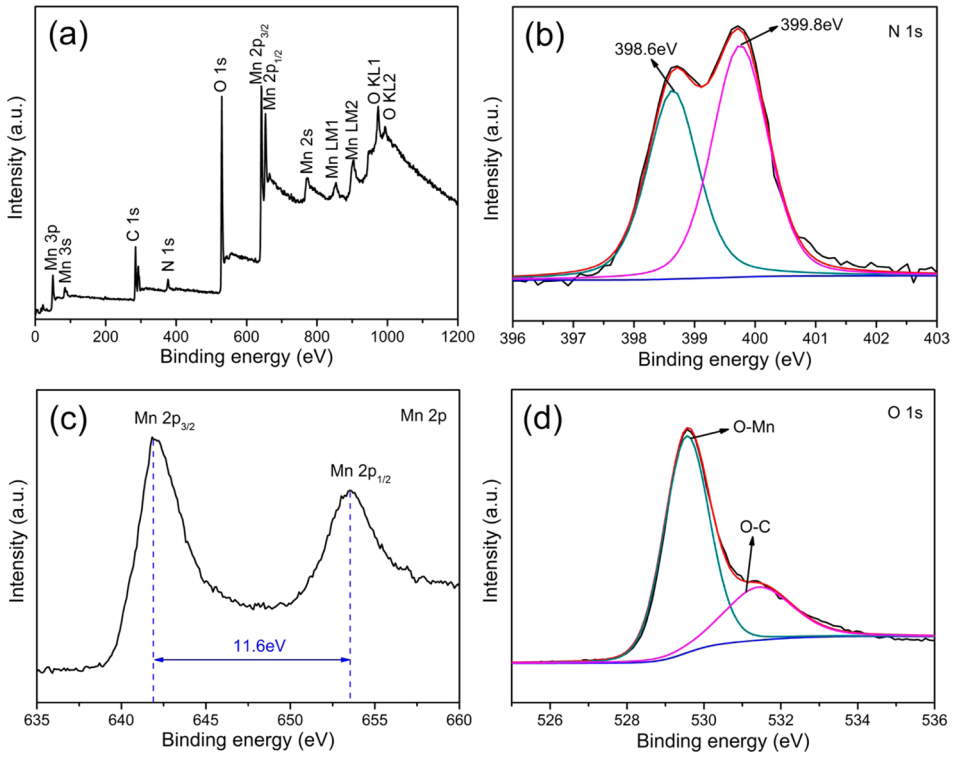

Figure 3. (a) XPS survey spectra of NGMCs, (b) the narrow spectra of N 1s, (c) the narrow spectra of Mn 2p, (d) the narrow spectra of O 1s.

M Na_2SO_4 aqueous solution within a potential window from 0 to 1 V (vs SCE). The CV curves are fairly rectangular shape, indicating that the composite electrode possesses perfect capacitive behavior. The galvanostatic charge/discharge curves of NGMCs at different current densities are shown in Figure 4b. The highly symmetrical charge/discharge curves indicate the excellent electrochemical reversibility during the charge/discharge processes. Furthermore, the potential drop (*iR* drop) is too small and can be ignored in all curves. From these curves, the specific capacitance (C) of the electrode can be calculated according to the following equation:[18] $C = I\Delta t/\Delta Vm$, where Δt is the discharge time, I is the discharge current, ΔV is the potential change during the discharge, and m represents the mass of active material in a NGMCs electrode. The specific capacitances calculated at 0.2, 0.5, 1, and 2 A/g are 257.1, 224.4, 205.6, and 192.5 F/g, respectively.

For comparison, the CV and galvanostatic charging/discharging measurements of GMCs were also performed. Figure 4c shows the CV curves of both NGMCs and GMCs at a scan rate of 20 mV/s. Since C is proportional to the areas of CVs, the results in Figure 4c reveal that C of NGMCs is superior to that of GMCs. The rectangular and symmetric CV curve of NGMCs indicates the ideal capacitive nature, whereas the CV curve of GMCs shows the lack of symmetry due to the aggregation of MnO_2 sheets on graphene surfaces.[7] Figure 4d shows galvanostatic charging/discharging curves for NGMCs and GMCs at 2 A/g. The longer discharging time of NGMCs represents the higher capacitance than that of GMCs. In addition, the *iR* drop of NGMCs is obviously smaller than that of GMCs, demonstrating that nitrogen doping increases the electrical conductivity of graphene due to the introduction of pyrrolic nitrogen and pyridinic nitrogen as reported previously.[41] Plots of the specific capacitance versus the current density are shown in Figure 4e. Approximately 74.9% (192.5 F/g) of the initial capacitance (257.1 F/g) for NGMCs is retained when the current density increases from 0.2 to 2 A/g. However, the GMCs retain only 27% at 2 A/g. The higher capacitance retention ratio of NGMCs can be attributed to synergetic effect of higher conductivity of NGMCs and well-dispersed ultrathin MnO_2 sheets. The electrochemical impedance spectroscopy (EIS) spectra for NGMCs and GMCs were shown in Figure S6 in the Supporting Information. According to analysis of Nyquist plots, the NGMCs display a lower charge-transfer resistance, indicating NGMCs possess an excellent conductivity. The improvement of the electrode conductivity can be attributed to the introduction of nitrogen atoms into graphene, which is consistent with the previous finding that N doping simultaneously increases the electrical conductivity and electrochemical activity of graphene in electrochemical process.[41] Moreover, well-dispersed ultrathin MnO_2 sheets can be confirmed by the larger specific surface area (158.74 $m^2\ g^{-1}$), as shown in Figure S7 in the Supporting Information, which allows the electrolyte to effectively interact with the active materials. Figure 4f shows the cycling stability of the NGMCs electrode and the GMCs electrode at a current density of 0.2 A/g in Na_2SO_4 solution between 0 and 1 V. It is found that the capacitance retention of 94.2% (242.2 F/g) was achieved for the NGMCs electrode, whereas the GMCs electrode retained ~82.1% (179.7 F/g) of the initial capacitance after 2000 cycles, which demonstrates that the NGMCs have better stability than the GMCs electrode.

CONCLUSIONS

In summary, nitrogen-doped graphene−ultrathin MnO_2 sheets composites (NGMCs) were prepared through a one-step hydrothermal method at low temperature (120 °C). The well-dispersed MnO_2 sheets with widths of 3−10 nm tightly anchored on doped graphene sheets. NGMCs electrode exhibited enhanced capacitive performances than those of

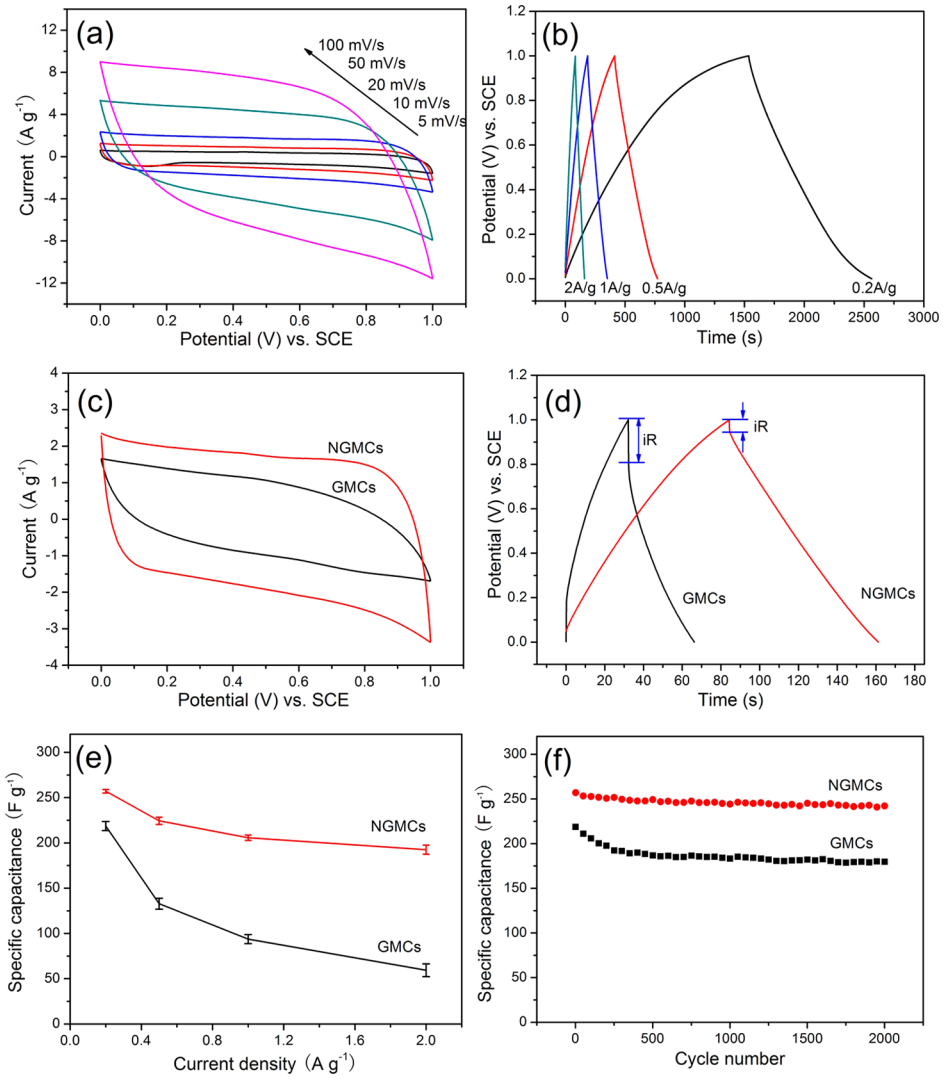

Figure 4. (a) CV of NGMCs at different scan rates, (b) galvanostatic charging/discharging curves of NGMCs at different current densities, (c) CV curves of NGMCs and GMCs at 20 mV/s, (d) galvanostatic charging/discharging curves for NGMCs and GMCs at 2 A/g, (e) effect of current density on the specific capacitance of NGMCs and GMCs, (f) cycle life of NGMCs and GMCs at 0.2 A/g in 1 M Na_2SO_4 solution.

undoped graphene-ultrathin MnO_2 sheets composites (GMCs), which resulted from the enhanced conductivity and superior dispersion of MnO_2 nanosheets on nitrogen-doped graphene upon N doping. As the current density was increased from 0.2 to 2 A/g, the capacitance of NGMCs still retained ~74.9%, significantly larger than that of GMCs (27%). Additionally, over 94.2% of the original capacitance was retained after 2000 cycles, indicating a good cycle stability of NGMCs electrode materials. This facile synthetic route has the potential to be developed as an effective method for the preparation of NG-based composite materials with superior electrochemical properties.

■ ASSOCIATED CONTENT

Supporting Information

TEM image of NGMCs and GMCs, SAED pattern of NGMCs, XPS survey spectra of GMCs, and TGA curves of NGMCs and NG. This material is available free of charge via the Internet at http://pubs.acs.org.

■ AUTHOR INFORMATION

Corresponding Author

*E-mail: liangao@mail.sic.ac.cn (L.G.); songxfeng@sjtu.edu.cn (X.S.). Fax: +86-21-52413122; Tel: +86-12-52412718.

Notes

The authors declare no competing financial interest.

■ ACKNOWLEDGMENTS

The authors greatly acknowledge the financial support by the Shanghai Municipal Natural Science Foundation (12ZR1414300), the National Natural Science Foundation of China (51172142), the Starting Foundation for New Teacher of Shanghai Jiao Tong University (12 × 100040119) and the Third Phase of 211 Project for Advanced Materials Science (WS3116205007).

■ REFERENCES

(1) Cericola, D.; Koetz, R. *Electrochim. Acta* **2012**, *72*, 1−17.
(2) Wang, G.; Zhang, L.; Zhang, J. *Chem. Soc. Rev.* **2012**, *41*, 797−828.
(3) Simon, P.; Gogotsi, Y. *Nat. Mater.* **2008**, *7*, 845−854.

(4) Hou, Y.; Cheng, Y.; Hobson, T.; Liu, J. *Nano Lett.* **2010**, *10*, 2727−2733.
(5) Yan, D.; Guo, Z.; Zhu, G.; Yu, Z.; Xu, H.; Yu, A. *J. Power Sources* **2012**, *199*, 409−412.
(6) Yuan, L.; Lu, X. H.; Xiao, X.; Zhai, T.; Dai, J.; Zhang, F.; Hu, B.; Wang, X.; Gong, L.; Chen, J.; Hu, C.; Tong, Y.; Zhou, J.; Wang, Z. L. *ACS Nano* **2012**, *6*, 656−661.
(7) Ragupathy, P.; Vasan, H. N.; Munichandraiah, N. *J. Electrochem. Soc.* **2008**, *155*, A34−A40.
(8) Liu, J.; Jiang, J.; Cheng, C.; Li, H.; Zhang, J.; Gong, H.; Fan, H. J. *Adv. Mater.* **2011**, *23*, 2076−2081.
(9) Song, M. K.; Cheng, S.; Chen, H.; Qin, W.; Nam, K. W.; Xu, S.; Yang, X. Q.; Bongiorno, A.; Lee, J.; Bai, J.; Tyson, T. A.; Cho, J.; Liu, M. *Nano Lett.* **2012**, *12*, 3483−3490.
(10) Yan, J.; Fan, Z.; Wei, T.; Qian, W.; Zhang, M.; Wei, F. *Carbon* **2010**, *48*, 3825−3833.
(11) Fan, Z.; Yan, J.; Wei, T.; Zhi, L.; Ning, G.; Li, T.; Wei, F. *Adv. Funct. Mater.* **2011**, *21*, 2366−2375.
(12) Yu, G.; Hu, L.; Liu, N.; Wang, H.; Vosgueritchian, M.; Yang, Y.; Cui, Y.; Bao, Z. *Nano Lett.* **2011**, *11*, 4438−4442.
(13) Wang, J. G.; Yang, Y.; Huang, Z. H.; Kang, F. *Electrochim. Acta* **2012**, *75*, 213−219.
(14) Eda, G.; Fanchini, G.; Chhowalla, M. *Nat. Nanotechnol.* **2008**, *3*, 270−274.
(15) Chun Hung, L.; Li, L.; Kin Fai, M.; Flynn, G. W.; Heinz, T. F. *Nature* **2009**, *462*, 339−341.
(16) Geim, A. K. *Science* **2009**, *324*, 1530−1534.
(17) Zhan, D.; Yan, J.; Lai, L.; Ni, Z.; Liu, L.; Shen, Z. *Adv. Mater.* **2012**, *24*, 4055−4069.
(18) Chen, S.; Zhu, J.; Wu, X.; Han, Q.; Wang, X. *ACS Nano* **2010**, *4*, 2822−2830.
(19) Zhu, J.; He, J. *ACS Appl. Mater. Interfaces* **2012**, *4*, 1770−1776.
(20) Liu, N.; Luo, F.; Wu, H.; Liu, Y.; Zhang, C.; Chen, J. *Adv. Funct. Mater.* **2008**, *18*, 1518−1525.
(21) Shao, Y.; Zhang, S.; Engelhard, M. H.; Li, G.; Shao, G.; Wang, Y.; Liu, J.; Aksay, I. A.; Lin, Y. *J. Mater. Chem.* **2010**, *20*, 7491−7496.
(22) Wang, H.; Wang, Q.; Cheng, Y.; Li, K.; Yao, Y.; Zhang, Q.; Dong, C.; Wang, P.; Schwingenschloegl, U.; Yang, W.; Zhang, X. X. *Nano Lett.* **2012**, *12*, 141−144.
(23) Wang, H.; Maiyalagan, T.; Wang, X. *ACS Catal.* **2012**, *2*, 781−794.
(24) Xinran, W.; Xiaolin, L.; Li, Z.; Youngki, Y.; Weber, P. K.; Hailiang, W.; Jing, G.; Hongjie, D. *Science* **2009**, *324*, 768−771.
(25) Mou, Z.; Chen, X.; Du, Y.; Wang, X.; Yang, P.; Wang, S. *Appl. Surf. Sci.* **2011**, *258*, 1704−1710.
(26) Lei, Z.; Lu, L.; Zhao, X. S. *Energy Environ. Sci.* **2012**, *5*, 6391−6399.
(27) Hulicova - Jurcakova, D.; Kodama, M.; Shiraishi, S.; Hatori, H.; Zhu, Z. H.; Lu, G. Q. *Adv. Funct. Mater.* **2009**, *19*, 1800−1809.
(28) Strelko, V.; Kuts, V.; Thrower, P. *Carbon* **2000**, *38*, 1499−1503.
(29) Chang, J.; Xu, H.; Sun, J.; Gao, L. *J. Mater. Chem.* **2012**, *22*, 11146−11150.
(30) Xu, Y.; Sheng, K.; Li, C.; Shi, G. *ACS Nano* **2010**, *4*, 4324−4330.
(31) Toupin, M.; Brousse, T.; Belanger, D. *Chem. Mater.* **2004**, *16*, 3184−3190.
(32) Ferrari, A.; Meyer, J.; Scardaci, V.; Casiraghi, C.; Lazzeri, M.; Mauri, F.; Piscanec, S.; Jiang, D.; Novoselov, K.; Roth, S. *Phys. Rev. Lett.* **2006**, *97*, 187401−187404.
(33) Jin, Z.; Yao, J.; Kittrell, C.; Tour, J. M. *ACS Nano* **2011**, *5*, 4112−4117.
(34) Luo, Z.; Lim, S.; Tian, Z.; Shang, J.; Lai, L.; MacDonald, B.; Fu, C.; Shen, Z.; Yu, T.; Lin, J. *J. Mater. Chem.* **2011**, *21*, 8038−8044.
(35) Jeong, H. M.; Lee, J. W.; Shin, W. H.; Choi, Y. J.; Shin, H. J.; Kang, J. K.; Choi, J. W. *Nano Lett.* **2011**, *11*, 2472−2477.
(36) Gong, K.; Du, F.; Xia, Z.; Durstock, M.; Dai, L. *Science* **2009**, *323*, 760−764.
(37) Chen, Z.; Higgins, D.; Chen, Z. *Carbon* **2010**, *48*, 3057−3065.
(38) Zheng, L.; Zhang, G.; Zhang, M.; Guo, S.; Liu, Z. H. *J. Power Sources* **2012**, *201*, 376−381.
(39) Hulicova, D.; Yamashita, J.; Soneda, Y.; Hatori, H.; Kodama, M. *Chem. Mater.* **2005**, *17*, 1241−1247.
(40) Qiu, Y.; Zhang, X.; Yang, S. *Phys. Chem. Chem. Phys.* **2011**, *13*, 12554−12558.
(41) Wu, Z. S.; Ren, W.; Xu, L.; Li, F.; Cheng, H. M. *ACS Nano* **2011**, *5*, 5463−5471.
(42) Tan, B. J.; Klabunde, K. J.; Sherwood, P. M. A. *J. Am. Chem. Soc.* **1991**, *113*, 855−861.
(43) Subramanian, V.; Zhu, H.; Vajtai, R.; Ajayan, P. M.; Wei, B. *J. Phys. Chem. B* **2005**, *109*, 20207−20214.
(44) Li, B.; Rong, G.; Xie, Y.; Huang, L.; Feng, C. *Inorg. Chem.* **2006**, *45*, 6404−6410.
(45) Huang, H.; Wang, X. *Nanoscale* **2011**, *3*, 3185−3191.
(46) Wu, Z. S.; Ren, W.; Wang, D. W.; Li, F.; Liu, B.; Cheng, H. M. *ACS Nano* **2010**, *4*, 5835−5842.
(47) Ma, W.; Zhou, J.; Lin, X. *Adv. Mater. Res.* **2011**, *287*−*290*, 539−543.
(48) Valles, C.; David Nunez, J.; Benito, A. M.; Maser, W. K. *Carbon* **2012**, *50*, 835−844.
(49) Yang, J.; Zhou, Y.; Sun, L.; Zhao, N.; Zang, C.; Cheng, X. *Appl. Surf. Sci.* **2012**, *258*, 5056−5060.
(50) Mao, L.; Zhang, K.; Chan, H. S. O.; Wu, J. *J. Mater. Chem.* **2012**, *22*, 1845−1851.